Desalination and Water Treatment
www.deswater.com
doi: 10.5004/dwt.2021.27000

220 (2021) 329–341
April

Comparative study of photocatalytic activity of nanocomposites prepared from biological wastes and ZnO nanoparticles

Chahrazed Djilani[a,c,*], Rachida Zaghdoudi[b,c], Fayçal Djazi[a,c], Abdelaziz Lallam[d], Bachir Bouchekima[e], Pierre Magri[f]

[a]*Faculté de Technologie, Université du 20 Août1955, B.P 26 Skikda 21000, Algeria, Tel. +213791665403; email: chahrazed_dj@yahoo.fr (C. Djilani)*
[b]*Faculté des Sciences, Université du 20 Août1955, B.P 26 Skikda 21000, Algeria, Tel. +213558872108; email: zeg_rach@yahoo.fr*
[c]*Laboratoire LRPCSI, Université du 20 Août1955, B.P 26 Skikda 21000, Algeria, Tel. +21377153129; email: djazi_faycal@yahoo.fr (F. Djazi)*
[d]*Laboratoire de Physique et Mécanique Textiles de l'ENSISA (LPMT), Université de Haute Alsace, 11 rue Alfred Werner, F 68093 Mulhouse CEDEX, France, Tel. +33389336900; email: abdelaziz.lallam@uha.fr*
[e]*Laboratoire de Développement des Energies Renouvelables (LENREZA), Université Kasdi Merbah, B.P 511 Ouargla 30000, Algeria, Tel. +213773725299; email:boucbachir@yahoo.fr*
[f]*LCP-A2MC, EA4164, Université de Lorraine, 1, bd Arago-57078 Metz, cedex3, France, Tel. +33387315433; email: pierre.magri@univ-lorraine.fr*

Received 5 August 2020; Accepted 5 January 2021

ABSTRACT

In this study, binary chitosan/zinc oxide (CS/ZnO) nanocomposite, ternary chitosan/activated carbon prepared from apricot stones/zinc oxide (CS/ACAS/ZnO) and chitosan/activated carbon prepared from animal bones/zinc oxide (CS/ACAB/ZnO) nanocomposites were synthesized for the comparative photocatalytic study of methylene blue dye in simulated contaminated water. The prepared CS/ZnO, CS/ACAS/ZnO and CS/ACAB/ZnO nanocomposites were systematically characterized using X-ray diffraction, Fourier-transform infrared spectroscopy and scanning electron microscopy. High rates of degradations were observed for CS/ACAS/ZnO (97%, 40 min) followed by CS/ACAB/ZnO (92%, 80 min) at initial pH, with an adsorbent dose of 100 mg at room temperature and for an initial concentration of 10 mg/L methylene blue. After comparison, the CS/ACAS/ZnO and CS/ACAB/ZnO nanocomposites exhibited the best photocatalytic performance for the methylene blue degradation under visible light irradiation. The kinetics of pseudo-first-order and pseudo-second-order models were checked to evaluate the photocatalytic performances of the considered nanocomposites. The results confirmed the successful incorporation of ZnO nanoparticles onto CS/ZnO, CS/ACAS/ZnO and CS/ACAB/ZnO and demonstrated that the use of activated carbons as a support for ZnO is a viable alternative and present a great interest for photocatalysis.

Keywords: Methylene blue; Zinc oxide; Nanocomposites; Photodegradation; Biological wastes

1. Introduction

Dyes are among the synthetic organic compounds which are widely used in the textile, leather, paint, paper, ink, printing, food, plastics and cosmetics industries. They are common pollutants in wastewaters due to their extensive use in various industries [1–3]. Dyeing waste showed highest level of toxicity followed by industrial waste, livestock waste and leather industrial waste [4]. Synthetic dyes are a significant class of organic pollutants that are released directly into the environment as wastewater from their

* Corresponding author.

industries [5]. This industrial wastewater enters the aquatic environment and leads to the generation of carcinogenic, cytogenetic, mutagenic, allergenic and toxic hazards for various organisms [6,7]. Dyes are typically classified into cationic dyes, anionic dyes and non-ionic dyes based on the charge of the chromophore group dissolved in the aqueous solution [8]. Methylene blue (MB) is a well-known cationic dye used as a colorant dye that is regularly applied for staining silk, wool, hemp, acrylic, cotton and as biological staining procedures [9,10]. The presence of MB in wastewater has some side effects, including burning eyes, nausea, diarrhea, and vomiting [2].

Several methods such as coagulation–flocculation aerobic or anaerobic treatment, electrochemical treatment, membrane filtration, photocatalytic degradation and adsorption have been adopted as prominent choices for the improvement of water quality through eliminating or removing dyes pollutants [11–16]. Adsorption has been found to be an efficient method for the removal of dyes from effluents, due to the effectiveness, high selectivity, easy-to-use, regeneration capability, low operating, non-toxicity and simplicity of the process [17,18]. Until now, many adsorbents such as activated carbons [19], magnetic carbon nanotubes [20] and composite hydrogels [21] have been successfully used for the removal of methylene blue from water. The principal disadvantage of adsorption methods is to create secondary pollution [22]. However, the photocatalysis method exhibits superior results for the removal of dyes and other complex pollutants from wastewater and environmental purification, in comparison with other techniques [1]. Compared with adsorption, the photocatalytic process is considered as one of the most promising and green technologies for eliminating organic contaminants because of its high efficiency for mineralization of dyes, the easy preparation of the catalyst, the absence of secondary pollution and finally the feasibility with light irradiation [23,24]. Consequently, the combination of adsorption and photocatalysis processes has been presented/introduced to enhance pollutant removal [25,26]. The photocatalysts and their photocatalytic performance for the degradation of organic dyes have been systematically investigated [27]. Generally, conventional non-porous semiconductor metal oxides, such as TiO_2, zinc oxide (ZnO), SnO_2, etc., are considered to be promising photocatalysts for complete degradation of organic pollutants to a friendly environment [28,29]. Among semiconductors, zinc oxide has the advantages of high chemical and physical stability, affordability, wide bandgap, large surface, UV-blocking ability, environmental friendly and biodegradation, which has been thoroughly studied in solar cells, adsorption and photo-catalysis [30–34]. ZnO has been considered for many applications, for example, ceramics, varistors, piezoelectric transducers, chemical sensors, anti-UV additives, photocatalysts, microwave absorbers, etc. [35]. The photocatalytic activity of ZnO is attributed to its wide band-gap of 3.37 eV and large excitonic binding energy of 60 meV at room temperature [36]. Some studies have confirmed that ZnO nanoparticles exhibit better efficiency than TiO_2 in photocatalytic degradation of some dyes [37]. Several researchers stated that the use of various combinations of ZnO with other materials such as TiO_2 [38], chitosan [39], zeolite [40], silica [41], carbon nanotube [42], graphene oxide [43] and activated carbon can improve the photocatalytic activity [44]. Activated carbon is a low-cost and non-toxic material that is considered an adsorbent for pollutant removal due to its high surface area, highly microporous structure, high catalytic activity, surface chemical properties and thermal stability [9,45]. Chitosan (CS) is a low cost renewable natural polymer characterized by perfect hydrophilicity, biocompatibility, biodegradability, non-toxicity, antimicrobial activity and activity for adsorbing toxic metals and organic compounds [39,46]. It is produced from the deacetylation of chitin and has been used in various applications [47]. The modification of chitosan and activated carbon with nanomaterials, specifically metal oxides nanoparticles such as TiO_2 [48,49], CuO [50,51], Fe_3O_4 [52,53] and ZnO [54,55] has gained great attention in the last decades as a result of the great value-added to their properties.

The study was aimed: (1) to prepare novel chitosan/activated carbons/ZnO nanocomposites; (2) to ameliorate the photocatalytic activity of CS/ZnO with the combination of activated carbons prepared from biological wastes; (3) to investigate by studying the degradation of methylene blue (as a model pollutant) under visible light irradiation.

2. Materials and methods

2.1. Materials

Commercial zinc oxide nanoparticles (ZnO) were purchased from Sigma-Aldrich, sodium hydroxide (NaOH, CAS: 1310-73-2, Mw = 40 g mol^{-1}, Biochem Chemopharma), hydrochloric acid (HCl, CAS: 7647-01-0, Mw = 36.46 g mol^{-1}, 37%, Sigma-Aldrich), hydrogen peroxide (H_2O_2, CAS: 7722-84-1, Mw = 34.02 g mol^{-1}, 30%, Biochem Chemopharma), acetic acid solution ($C_2H_4O_2$, CAS: 64-19-7, Mw = 60.05 g mol^{-1}, 99%, Sigma-Aldrich), nitric acid (HNO_3, CAS: 7697-37-2, Mw = 63.01 g mol^{-1}, 65%, Chem-Lab), phosphoric acid (H_3PO_4, CAS: 7664-38-2, Mw = 98 g mol^{-1}, 95%, Sigma-Aldrich), potassium hydroxide (KOH, CAS: 1310-58-3, Mw = 56.11 g mol^{-1}, Biochem Chemopharma), methylene blue (MB, molecular formula is $C_{16}H_{18}ClN_3S$, C.I. No.52015, Mw = 319.85 g mol^{-1}, Biochem Chemopharma).

2.2. Preparation of CS, ACAS and ACAB adsorbents

In this work, commercially pure zinc oxide, chitosan prepared from shrimp shells and two prepared activated carbons from apricot stones and animal bones, with different physical and chemical properties, were used.

The preparation method of chitosan (CS), activated carbon prepared from apricot stones (ACAS) and activated carbon prepared from animal bones (ACAB) was prepared according to a literature method [56–58].

The shrimp shells were washed thoroughly with flowing tap water to remove the soil and extraneous matter, dried and eventually ground into powders using a commercial grinder. Chitin was prepared from shrimp shells waste by a chemical process involving deproteination (NaOH, 2.5 M, 75°C, 6 h), demineralization (HCl, 1.7 M, room temperature, 6 h) and decolorization (H_2O_2, 20%). Chitosan was prepared from chitin by deacetylation (NaOH, 50%, 100°C, 6 h).

Local apricot stones, which are a by-product of food processing, were collected and washed in distilled water. The apricot stones were crushed and ground in the laboratory. The carbonization was carried out by loading 10 g of dried apricot stones into a muffle furnace and heated a carbonization temperature of 700°C for 1 h. The modification of the carbonized material was done by mixing 10 g of sample with 250 mL of a mixture of 70% H_3PO_4 + HNO_3. After activation, the activated carbon prepared from apricot stones was washed with distilled water to remove residual chemicals and dried in an oven at 105°C for 24 h. The ACAS was ground and sieved to the required particle size (150–250 μm).

Bovine bones were collected from a local butcher. The bones were carefully washed with water severally and well cleaned from meat and fat. The dried bovine bones were crushed to a fine powder in an electrical grinder then calcined for 2 h at 700°C. The calcined material was impregnated with the KOH solution (0.01 M) and the activation step was carried out in glass tubes placed in a microwave. The microwave power was adjusted at 600 W for an irradiation time of 20 min. Activated carbon from bovine bones was washed using distilled water and dried in an oven at 105°C for 24 h.

2.3. Preparation of CS/ZnO, CS/ACAS/ZnO and CS/ACAB/ZnO NCs

CS/ACAS/ZnO and CS/ACAB/ZnO solutions were obtained by dissolving 1 g of ZnO powder in 100 mL of 1% acetic acid where it changed to zinc cations, then 1 g of chitosan (CS) was added to the mixture solution. The solution was mixed for about 10 min and then 1 g of activated carbon powder was added and mixed vigorously and sonicated for 30 min at room temperature. Then, 1 M NaOH was added drop by drop under magnetic stirring until the solution reached a pH value of 10. The mixture was heated in a water bath at 80°C for about 3 h. Finally, the resulting solution was filtered and washed with distilled water several times then dried in an oven at 80°C for 3 h forming CS/ACAS/ZnO and CS/ACAB/ZnO nanocomposites. The nanocomposite CS/ZnO was prepared in a similar way by using 1 g CS and 1 g ZnO [59].

2.4. Characterization methods

The crystal structures of ZnO, CS/ZnO, CS/ACAS/ZnO and CS/ACAB/ZnO were analyzed using a Bruker diffractometer, model D8 ADVANCE, equipped with a CuKa source and a fast detector LYNXEYE (systemθ-θ) and working at the monochromatic radiation $K\alpha_1$ wavelength of copper (λ = 1.5406 Å). The JCPDS PDF database was used for phase identification.

The surface chemistry of CS, ACAS, ACAB, ZnO, CS/ZnO, CS/ACAS/ZnO and CS/ACAB/ZnO was evaluated by Fourier-transform infrared spectroscopy (FTIR) spectrometer (FTIR-8400S SHIMADZU). The spectra were recorded in the frequency range of 650–4,000 cm^{-1}.

The microstructure and morphology of CS, ACAS, ACAB, ZnO, CS/ZnO, CS/ACAS/ZnO and CS/ACAB/ZnO were examined using a scanning electron microscope (HITACHI S-2360 N). Scanning electron microscopy (SEM) experiment was conducted at an accelerator voltage range of 20–22 kV. Micrographs of the nanocomposites were performed with different magnifications of 300×, 600× and 3,000×.

The surface area of the nanocomposites was determined via the method described by Rao et al. [60]. After this, 0.5 g of adsorbent was placed in biochemical oxygen demand bottles containing 50 mL of 0.015, 0.025, 0.05, 0.10 and 0.15 M acetic acid. A control sample was also prepared for each concentration that did not contain any adsorbent. These samples were tightly closed and agitated for 1 h at 150 rpm before being filtered using 0.45-μm filter paper. The filtrate was titrated with a standard NaOH (0.1 mol L^{-1}) solution to determine the remaining concentration of acetic acid (C). The concentration of acetic acid remaining in each case (C) was divided by the number of moles of acetic acid (N) adsorbed per gram of adsorbent to determine the C/N ratio. The slope of the linear plot of C/N vs. C yielded N_m (N_m = 1/slope). By substituting N_m into the following equation, the surface area, A (m^2 g^{-1}), can be calculated using:

$$A = N_m \times N_0 \times \sigma \times 10^{-20} \quad (1)$$

where N_0 is Avogadro's number, N_m is the number of moles per gram required to form a monolayer and σ is the molecular cross-sectional area given by a square Angstrom (21 Å) for acetic acid.

2.5. Photocatalytic activity

The photocatalytic activity of all nanocomposites (CS/ZnO, CS/ACAS/ZnO and CS/ACAB/ZnO) was confirmed by the removal of methylene blue (MB) from the aqueous solution. Typically, 0.1 g of CS/ZnO nanocomposite was added to 50 mL of 10 mg L^{-1} MB solution and the resulting solution was placed in a quartz vessel to form a suspension under stirring. The suspensions were stirred first in the dark for 45 min to evaluate the adsorption/desorption equilibrium between the MB and the surface of the CS/ZnO nanocomposite. The suspension was then exposed to visible light (LED lamp 5 W) for the required time. During irradiation, the samples were withdrawn from the solution at fixed time intervals. Centrifugation of the samples was proceeded to eliminate the presence of any solid particles and measured with UV-Vis spectrophotometer (SHIMADZU UV-1700) at wavelengths at 665 nm for MB. The photocatalytic degradation of CS/ACAS/ZnO and CS/ACAB/ZnO was carried out using a similar process.

The degradation efficiency of MB by the nanocomposites CS/ZnO, CS/ACAS/ZnO and CS/ACAB/ZnO was then evaluated by calculating the percent of degradation using the following equation:

$$D(\%) = \frac{C_0 - C_t}{C_0} \times 100 \quad (2)$$

where C_0 is the initial concentration of MB and C_t is its concentration after irradiation time (t).

In this study, the kinetics of the photodegradation of MB using the prepared nanocomposites corresponding to the kinetic of pseudo-first-order (Langmuir–Hinshelwood model) and pseudo-second-order models were studied to evaluate the photocatalytic performances of the considered nanocomposites [31].

In the pseudo-first-order kinetic model, the relationship between $\ln(C_0/C_t)$ and t can be expressed as follows:

$$\ln\left(\frac{C_0}{C_t}\right) = k_1 t \tag{3}$$

While in the pseudo-second-order kinetic model, the relationship between $(1/C_t - 1/C_0)$ and t can be expressed as follows:

$$\frac{1}{C_t} - \frac{1}{C_0} = k_2 t \tag{4}$$

where C_0 is the initial concentration of MB, C_t is the current concentration of MB, k_1 (min^{-1}) is the photodegradation rate constant of the first-order model and k_2 (L mg^{-1} min^{-1}) is the photodegradation rate constant of the second-order model.

3. Results and discussion

3.1. X-ray diffraction, FTIR and SEM of materials

The crystal structure of the nanocomposites was confirmed using X-ray diffraction (XRD) analysis. The X-ray diffraction patterns of ZnO, CS/ZnO, CS/ACAS/ZnO and CS/ACAB/ZnO were collected in the 2θ range from 10° to 80°.

The X-ray diffraction pattern of the commercial ZnO nanoparticles is depicted in Fig. 1. The results reveal that the ZnO exhibits hexagonal structure and the peaks are in accordance with the standard data (JCPDS file n°89-1397). The crystal size of ZnO sample was estimated using width tapes XRD pattern and Scherrer's Eq. (5) [61]:

$$D = \frac{K\lambda}{\beta\cos\theta} \tag{5}$$

where D is the crystalline particle size in terms of nm, K is Scherrer constant (0.9), λ is the wavelength of X-ray (0.154 nm), β is the full-width half-maximum of intensity and θ is the Bragg's angle.

The average crystallite size value is approximately 65 nm. The lattice parameters are found to be a = 3.2417 Å and c = 5.1876 Å. Similarly, the space group of the commercial ZnO sample is found to be P63mc.

The XRD profiles, associated in Figs. 2a–c, of CS/ZnO, CS/ACAS/ZnO and CS/ACAB/ZnO show the presence of characteristic diffraction peaks at 2θ values of 31.7°, 34.4°, 36.1°, 47.4°, 56.6°, 62.8°, 66.3°, 68° and 69°, corresponding to the diffraction planes of (100), (002), (101), (102), (110), (103), (200), (112), and (201), respectively, confirming the Hexagonal Wurtzite structure of ZnO nanoparticles, which are in very good agreement with the standard JCPDS file n°89-1397 for ZnO. Similar observations were reported in previous studies [6,45,62,63].

The characteristic peak at 2θ = 20° is originated from the amorphous structure of chitosan [64]. The XRD patterns of ACAS and ACAB present no peaks confirming its amorphous structure. The amorphous structure of activated carbons is clearly dominant in the CS/ACAS/ZnO and CS/ACAB/ZnO nanocomposites. XRD peaks of ZnO are visible in this nanocomposite confirming the presence of ZnO in crystalline stage in all the nanocomposites. This suggests that the crystal structure of ZnO nanoparticles has not been modified due to the presence of CS, ACAS and ACAB (may be due to chemical bonds).

The surface functional groups of the adsorbents (CS, ACAS, ACAB), nanoparticles (ZnO) and nanocomposites (CS/ZnO, CS/ACAS/ZnO, CS/ACAB/ZnO) is confirmed by the FTIR spectral analysis. The FTIR spectra of CS, ACAS, ACAB, ZnO, CS/ZnO, CS/ACAS/ZnO, and CS/ACAB/ZnO are shown in Figs. 3 and 4.

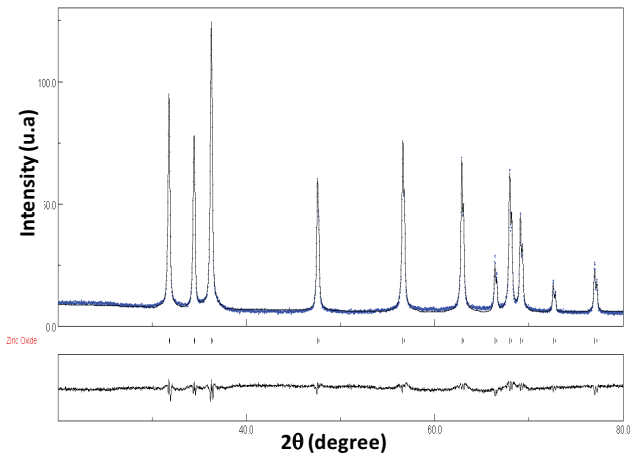

Fig. 1. Rietveld refinement of the XRD pattern of the ZnO. Experimental (blue line) and calculated (black line).

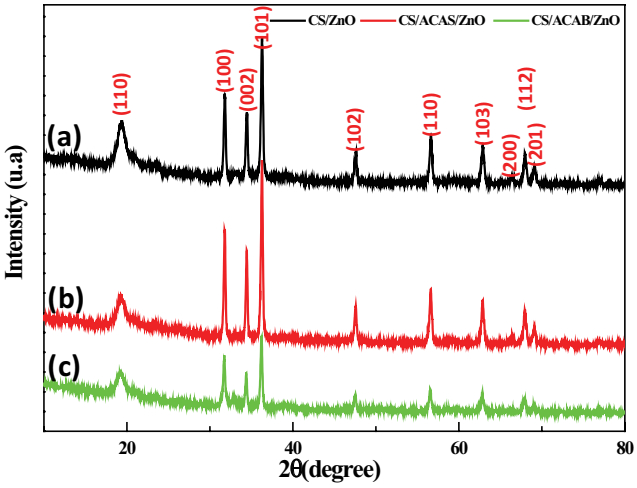

Fig. 2. XRD analysis of (a) CS/ZnO, (b) CS/ACAS/ZnO and (c) CS/ACAB/ZnO nanocomposites.

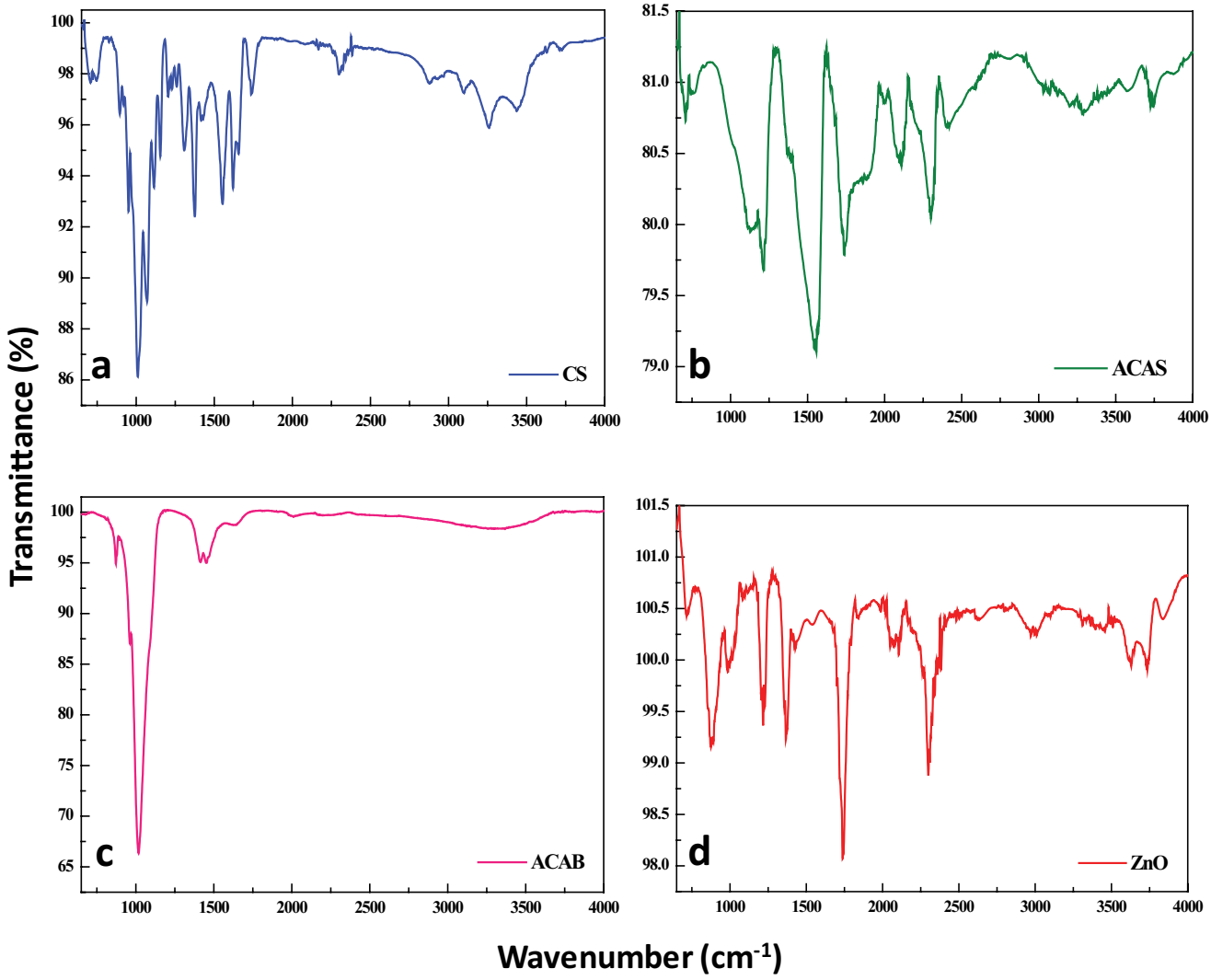

Fig. 3. FTIR spectra of (a) CS, (b) ACAS, (c) ACAB and (d) ZnO.

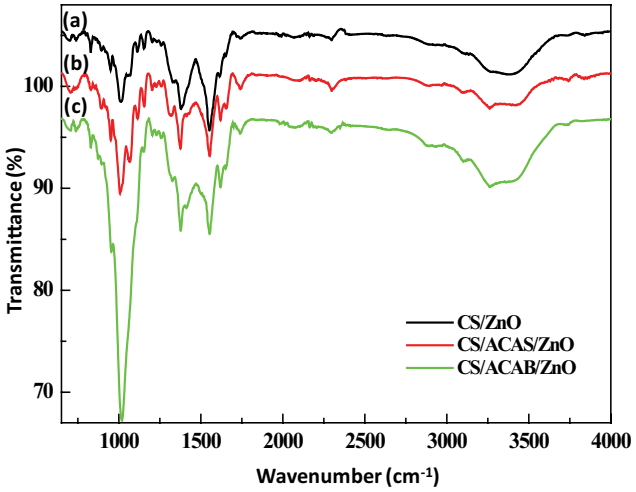

Fig. 4. FTIR spectra of (a) CS/ZnO, (b) CS/ACAS/ZnO and (c) CS/ACAB/ZnO nanocomposites.

The obtained FTIR spectrum of CS (Fig. 3a) reveal the presence of peaks located at 3,435; 2,872; 1,619; 1,553; 1,375; 1,041 and 880 cm^{-1} corresponding to the presence of O–H and N–H symmetric stretching vibration, C–H stretching vibration of the aliphatic, N–H bending vibrations of the primary amine group of CS, N–H bending of secondary amine, C–N stretching vibration, C–O stretching vibration and γ(C–H) in the aromatic ring [56].

The spectrum of ACAS (Fig. 3b) indicates the existence of peaks located at 3,294–3,751; 2,303; 1,739; 1,548; 1,219 and 1,131 cm^{-1}, identical to the presence of O–H stretching vibration, C≡C stretching vibration of alkyne groups, C=O stretching vibration, C=C stretching vibration, aromatic CO– and phenolic –OH, and stretching vibrations of C–O in volatile species and carboxyl acids [57,65].

Many bands in the spectra of ACAB (3,352; 1,454; 1,018 and 870 cm^{-1}) are in good agreement with the literature data on hydroxyapatite (Fig. 3c) [58].

In the ZnO nanoparticles (Fig. 3d), there exist bands at 3,382–3,735; 2,990; 2,303; 1,749; 1,440 and 880 cm^{-1} which

could be associated with the presence of δ(–OH), δ(C–H), δ(C–O), δ(C–O), δ(C–O) and ϑ(C–H), respectively [66,67].

Comparing the FTIR spectra of the prepared nanocomposites CS/ZnO, CS/ACAS/ZnO and CS/ACAB/ZnO (Figs. 4a–c), it can be noticed that the main vibration modes of CS, ACAS, ACAB and ZnO can be observed in the FTIR spectra of CS/ZnO, CS/ACAS/ZnO and CS/ACAB/ZnO. The FTIR spectrum of the CS/ZnO nanocomposite indicates the presence of the characteristic peaks which are related to the chitosan and ZnO.

In comparison with CS, the increase in the intensity of CS/ZnO at the band range of 3,362 cm^{-1} suggests the formation of new interactions between NH_2 and OH groups of CS and ZnO (Fig. 4a) [68,69]. Chitosan contains reactive amine and hydroxyl groups on its backbone that makes it act as a Lewis base and form coordination bonds with metal ions. The complexation reaction between CS and surface of ZnO nanoparticles occurs via ligand substitution reaction where the functional groups of CS substitute water molecules that are coordinated to surface zinc cations [39].

The same change was found in the band range of 1,383 cm^{-1} (COO–, C–N) and 1,538 cm^{-1} (C=C, N–H). The appearance of a band in the range of 871 cm^{-1} in the spectrum of CS/ZnO suggests the presence of ZnO [55,62].

Compared to the spectra of CS/ACAS/ZnO and CS/ACAB/ZnO with CS/ZnO (Figs. 4a–c), the broader and stronger peak shifted to low wavenumber at 3,261 and 3,266 cm^{-1} for ACAS and ACAB, respectively, which indicates a very strong interaction between the functional groups of CS, functional groups of activated carbons and the ZnO nanoparticles [70]. Thus, many changes in the absorption bands of CS/ACAS/ZnO and CS/ACAB/ZnO have been observed. Major absorption bands are observed between 650 and 1,900 cm^{-1}. They are a combination of several overlapping peaks and it is generally observed as a double band.

The increase in peak intensities is observed in CS/ACAS/ZnO (1,010; 1,739 and 2,297 cm^{-1}) and CS/ACAB/ZnO (1,021 cm and 1,370 cm^{-1}) as compared to CS/ZnO. It is an indication of the formation of coordination bonds between various groups of Chitosan, activated carbons and Zn^{2+} ions of nanoparticles [45,63]. Finally, the results revealed that the functional groups present on the surfaces of CS, ACAS, ACAB and ZnO were also identified on the CS/ZnO, CS/ACAB/ZnO and CS/ACAB/ZnO surfaces, hence, the nanocomposites were successfully formed.

The SEM images of CS, ACAS, ACAB, ZnO, CS/ZnO, CS/ACAS/ZnO and CS/ACAB/ZnO are given in Figs. 5 and 6. The micrographs (Figs. 5a and b) show a heterogeneous and relatively smooth structure for chitosan. The scanning electron micrographs of Figs. 5c and d indicate that the activated carbon prepared from apricot stones show the presence of porosity, irregularity and high heterogeneity compared to CS and ACAB. The images of the activated carbon prepared from the animal bones (Figs. 5e and f) reveal the irregular morphology of ACAB.

The surface morphologies of ZnO, CS/ZnO, CS/ACAS/ZnO and CS/ACAB/ZnO are compared in Figs. 6a–g. The SEM analysis is performed to study the significant changes in the surface morphology of the CS/ZnO, CS/ACAS/ZnO and CS/ACAB/ZnO in comparison to CS, ACAS, ACAB and ZnO. As can be seen from Figs. 6a and b, the ZnO nanoparticles have a crystalline spherical structure and uniform distribution. The SEM images of CS/ZnO, CS/ACAS/ZnO and CS/ACAB/ZnO (Figs. 6c–g) show the main difference between the nanocomposites prepared from CS, CS/ACAS and CS/ACAB which is the agglomeration and distribution of ZnO nanoparticles on the nanocomposites surfaces. The morphologies of CS, ACAS and ACAB have changed by the introduction of the ZnO nanoparticles. The surface morphology of the prepared nanocomposites reveals the spherical shape.

The specific surface areas of the CS/ZnO, CS/ACAS/ZnO and CS/ACAB/ZnO were 86.43 $m^2\ g^{-1}$ ($N_m = 0.6833 \times 10^{-3}$ mol g^{-1}), 330.76 $m^2\ g^{-1}$ ($N_m = 2.6151 \times 10^{-3}$ mol g^{-1}) and 251.36 $m^2\ g^{-1}$ ($N_m = 1.9873 \times 10^{-3}$ mol g^{-1}), respectively.

3.2. Kinetics study of the photodegradation of MB

In the dark, 26.8%, 36.1% and 67.5% of MB were adsorbed onto CS/ZnO, CS/ACAB/ZnO and CS/ACAS/ZnO in 45 min. This indicates a higher adsorption capacity of CS/ACAS/ZnO compared to CS/ZnO. CS/ZnO show a low adsorption capacity and it is due to the high percentage of ZnO compared with CS/ACAS/ZnO. The high specific surface area and the abundance of pore structures ensured the adsorption capacity of activated carbons for MB dye removal. This suggests that the presence of the activated carbons is mainly responsible for the methylene blue adsorption capability of the materials. These data reveal that the CS/ACAS/ZnO could be potentially used as adsorbent in the absence of visible light.

During irradiation, the photocatalytic degradation rate percentage of the MB solution can be easily calculated using Eq. (1) and the value is found to be 55% (CS/ZnO), 92% (CS/ACAB/ZnO) and 97% (CS/ACAS/ZnO) at 80, 80 and 40 min, respectively. It is evident from Fig. 7a that CS/ACAS/ZnO has the capability to almost fully degrade the MB dye within 40 min. However, CS/ACAB/ZnO is able to degrade 92% within 80 min.

The relatively high degradation rate of CS/ACAS/ZnO and CS/ACAB/ZnO can be attributed to the adsorption to MB during dark processing (Figs. 7a and b). It is found that light irradiation promoted the removal of MB by CS/ACAS/ZnO, indicating that CS/ACAS/ZnO was provided with certain photocatalytic ability. However, the rate of MB dye degradation was considerably improved after the incorporation of both ACAS and ACAB into the CS/ZnO matrix. This resultant was attributed to the small particle size, the large surface area of activated carbons ACAB and ACAS, rich functional groups and superior charge transfer from activated carbons to ZnO. Obviously, activated carbons combined on CS/ZnO significantly improved the MB degradation efficiency compared to CS/ZnO. Other researchers have adequately demonstrated that activated carbon with various surface groups offered photocatalytic activity [71].

In addition, the synergetic effect of photocatalysis and adsorption is the main reason for excellent MB degradation of the CS/ACAS/ZnO and CS/ACAB/ZnO nanocomposites.

Visible light is an energy that can be involved directly and is needed to activate the photocatalytic properties of the material to form radical species that contribute to the

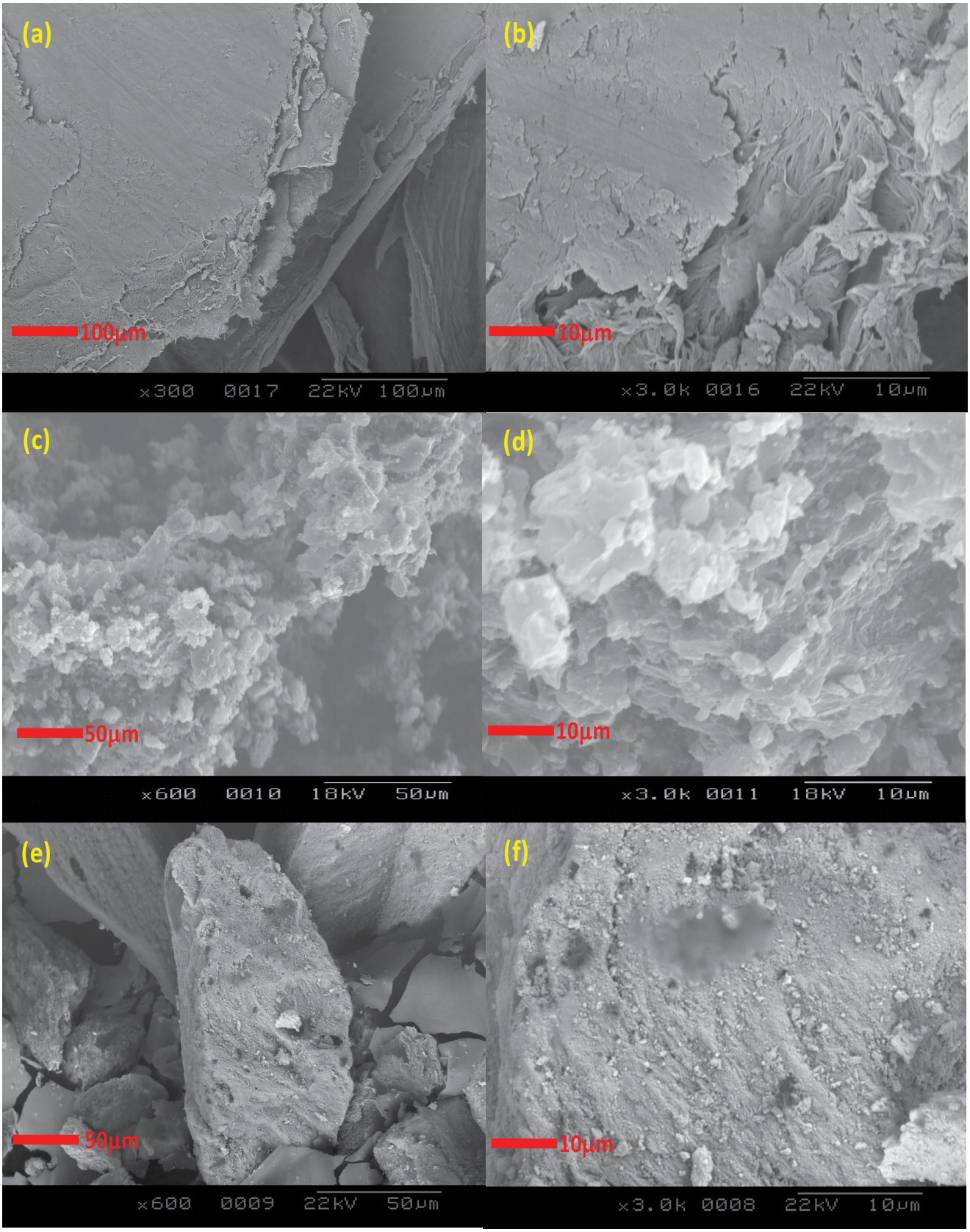

Fig. 5. SEM images of (a and b) CS, (c and d) ACAS and (e and f) ACAB at different magnifications.

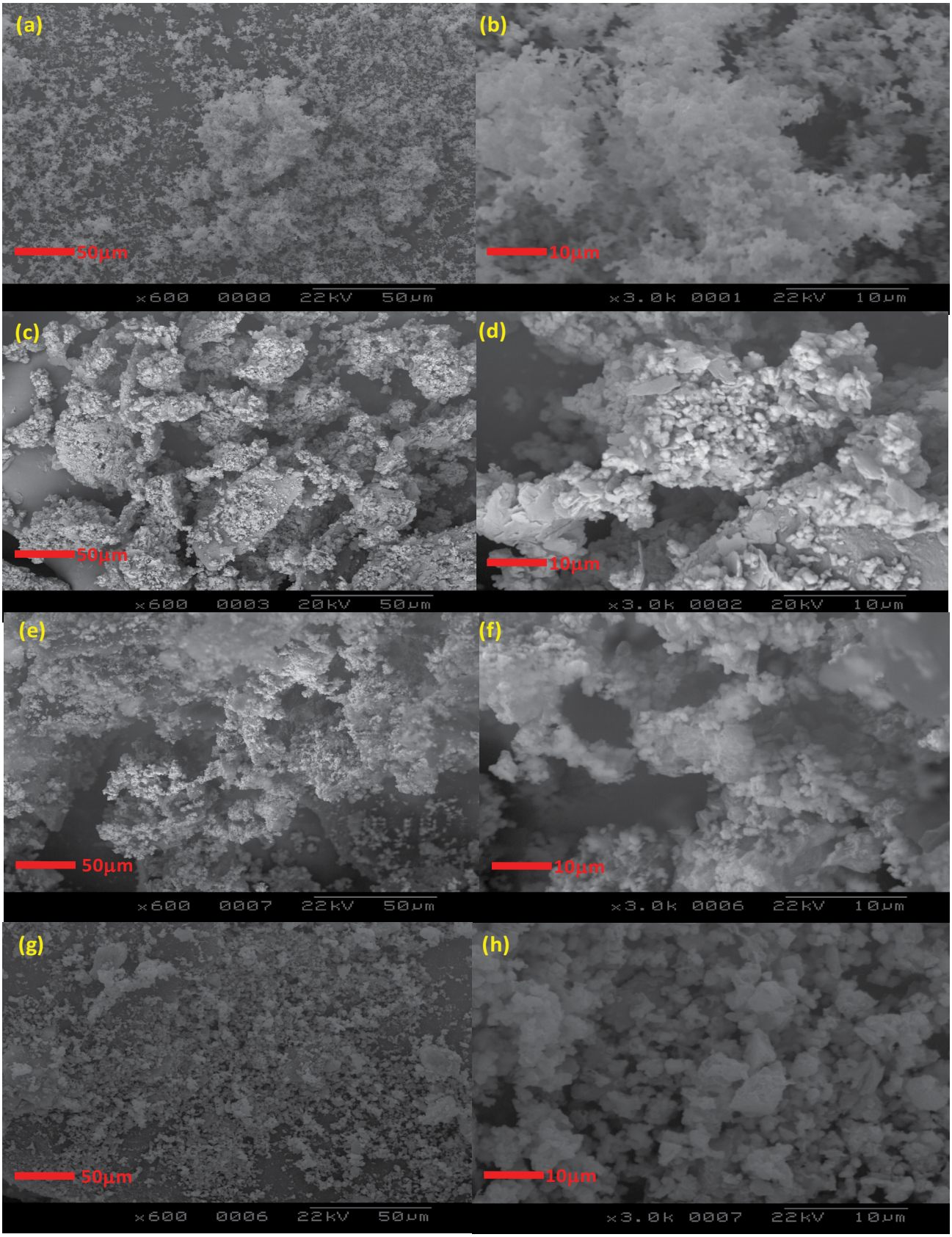

Fig. 6. SEM images of (a and b) ZnO, (c and d) CS/ZnO, (e and f) CS/ACAS/ZnO and (g and h) CS/ACAB/ZnO at different magnifications.

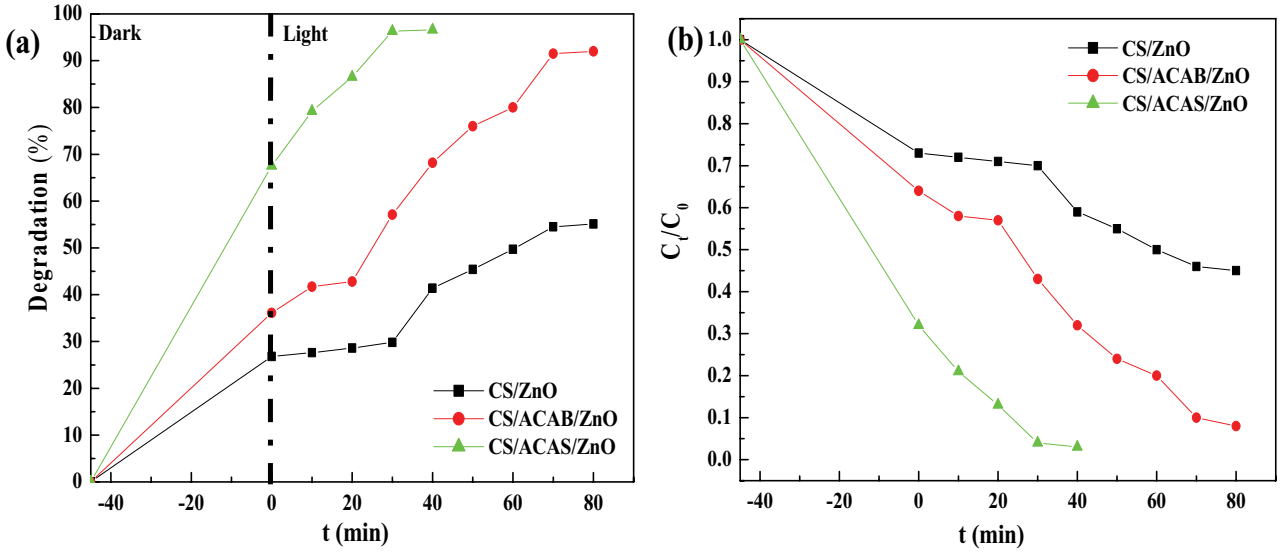

Fig. 7. (a) Decolorization of MB (b) process for the degradation of MB using CS/ZnO, CS/ACAB/ZnO and CS/ACAS/ZnO nanocomposites under dark and visible light (conditions: V = 50 mL; $m_{nanocomposite}$ = 100 mg; C_{MB} = 10 mg/L).

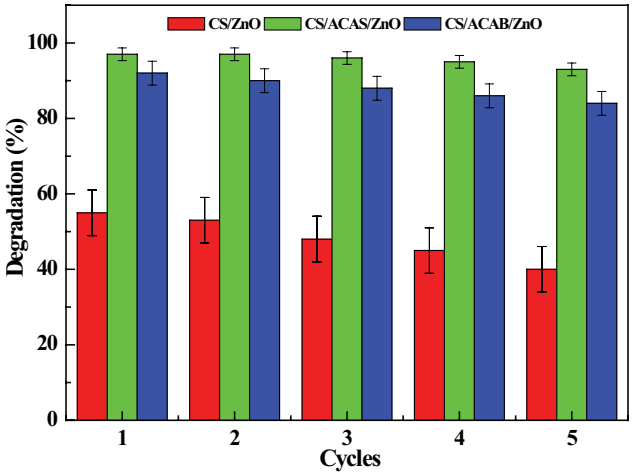

Fig. 8. Reusability of CS/ZnO, CS/ACAS/ZnO and CS/ACAB/ZnO up to 5 cycles.

degradation of the methylene blue dye into green compounds. The activated carbon could increase the photocatalytic performance of ZnO nanoparticles by promoting the effective charge separation of electron-hole pairs if they can be composited. Although the large holes of activated carbons have been occupied by ZnO nanoparticles, blocking the porosity of the activated carbons surface. Under the radiation of light, the holes (h+) generated in the valence bond (VB) of nanocomposites interact with either the hydroxyl groups adsorbed on the surface of nanocomposites or the water in the medium. As a result, hydroxyl radicals are produced which accelerates the degradation of the methylene blue. These results indicate that the CS/ACAB/ZnO and CS/ACAS/ZnO nanocomposites have a certain photocatalytic activity [72,73].

The photodegradation rate constant of the first-order model calculated from the slope of the best fit line of the plot of $\ln(C_0/C_t)$ vs. reaction time (t) and the value of the apparent rate constant of the second-order model can be estimated by calculating the slope of a plot between $(1/C_t - 1/C_0)$ vs. reaction time (t). The calculated rate constants are summarized in Table 1. The rate constants for the CS/ACAS/ZnO (0.0698 min^{-1}, 0.0754 L mg^{-1} min^{-1}) and CS/ACAB/ZnO (0.0109 min^{-1}, 0.0309 L mg^{-1} min^{-1}) are higher when compared to CS/ZnO (0.0016 min^{-1}, 0.0114 L mg^{-1} min^{-1}). The highest k_1 and k_2 in MB may be due to the synergistic effect of adsorption by activated carbons and the interaction between the surface of CS/ZnO, CS/ACAB/ZnO and CS/ACAS/ZnO nanocomposites and the MB structure. Generally, the photocatalytic reactions will happen by adsorption of the target molecule on the surface of photocatalyst which is followed by oxidation by •OH radical. The results indicate that the photodegradation of MB fits pseudo-first-order and pseudo-second-order degradation kinetics ($R^2 > 0.9$).

The photodegradation of MB for different nanocomposites containing ZnO nanoparticles are summarized in Table 2. Our result is in compliance with the other works (97% of CS/ACAS/ZnO, 92% of CS/ACAB/ZnO).

3.3. Reusability study

The regeneration or reuse of the nanocomposites are one of the significant economic factors in the water treatment process. The prepared nanocomposites were tested for its stability and reusability in the reduction MB dye under visible light irradiation. The reusability experiments were employed under the same conditions of original experiment. The applicability of using the nanocomposites for several cycles of MB dye degradation was investigated for five consecutive cycles and data presented in Fig. 8. The results revealed that CS/ACAS/ZnO nanocomposite retained its activity up to five successive runs without significant loss in its photocatalytic activity in

Table 1
Kinetic constant and correlation coefficient of MB degradation by all nanocomposites

Nanocomposites	Pseudo-first-order		Pseudo-second-order	
	k_1 (min^{-1})	R^2	k_2 (L mg^{-1} min^{-1})	R^2
CS/ZnO	0.0016	0.9665	0.0114	0.9690
CS/ACAB/ZnO	0.0109	0.9284	0.0309	0.9635
CS/ACAS/ZnO	0.0698	0.9380	0.0754	0.9269

Table 2
Comparison of photocatalytic activity between some photocatalyst contains ZnO nanoparticles

Samples	Dyes	Degradation (%)	References
Fe/ZnO@ceramic	Reactive Black 5	90	[74]
UV/H_2O_2/ZnO	Violet 26	90.1	[75]
ZnO/UV/H_2O_2	Disperse Red 60	97	[76]
ZnO/PUF	Acid Black 1	86	[77]
Ag/ZnO/G-C_3N_4	Methylene blue	98	[78]
Biochar-ZnO	Acid red 97	100	[79]
ZnO/SB450	Methyl orange	90.8	[80]
Ag/ZnO-montmorillonite	Methylene blue	82.5	[81]
CS/ZnO	Methylene blue	55	This work
CS/ACAS/ZnO	Methylene blue	97	This work
CS/ACAB/ZnO	Methylene blue	92	This work

the reduction of MB dye. It is suggested that CS/ACAS/ZnO nanocomposite may greatly contribute to solving the problems of dyes-polluted wastewater and water purification.

4. Conclusion

In this study, we developed an efficient photocatalysts composed of CS/ZnO with activated carbons prepared from biological wastes and investigated its comparative photodegradation for methylene blue onto CS/ZnO, CS/ACAS/ZnO and CS/ACAB/ZnO. The methylene blue was employed as a model dye to evaluate the photocatalytic degradation capability of the prepared nanocomposites under visible light irradiation in aqueous solution. The crystal structures, surface morphology and functional surface groups of the nanocomposites were characterized by XRD, FTIR and SEM. The XRD confirmed the presence of ZnO in crystalline stage in all the considered nanocomposites. The SEM images displayed agglomerated nanoparticles on the nanocomposites. The FTIR studies were in a good agreement with the XRD and SEM analyses. High rates of degradations were observed for CS/ACAS/ZnO (97%, 40 min) followed by CS/ACAB/ZnO (92%, 80 min) and CS/ZnO (55%, 80 min), respectively. The CS/ACAS/ZnO nanocomposite showed excellent adsorption properties with a high removal capacity of methylene blue of about ~68% in 45 min. The results showed that the nanocomposites prepared from chitosan, activated carbons and ZnO exhibited superior performance compared to chitosan and ZnO-based nanocomposites. The combination of activated carbons with a CS/ZnO blend improved its adsorption capacity and photocatalytic performance. The CS/ACAS/ZnO nanocomposite exhibited superior adsorption and photocatalytic degradation of methylene blue dye.

References

[1] S. Singhal, S. Dixit, A.K. Shukla, Self-assembly of the Ag deposited ZnO/carbon nanospheres: a resourceful photocatalyst for efficient photocatalytic degradation of methylene blue dye in water, Adv. Powder Technol., 29 (2018) 3483–3492.
[2] M. Nadimi, A.Z. Saravani, M.A. Aroon, A.E. Pirbazari, Photodegradation of methylene blue by a ternary magnetic TiO_2/Fe_3O_4/graphene oxide nanocomposite under visible light, Mater. Chem. Phys., 2251 (2019) 464–474.
[3] N. Masoudian, M. Rajabi, M. Ghaedi, Titanium oxide nanoparticles loaded onto activated carbon prepared from bio-waste watermelon rind for the efficient ultrasonic-assisted adsorption of congo red and phenol red dyes from wastewaters, Polyhedron, 173 (2019) 114105, https://doi.org/10.1016/j.poly.2019.114105.
[4] M. Abbas, M. Adil, S. Ehtisham-ul-Haque, B. Munir, M. Yameen, A. Ghaffar, G.A. Shar, M.A. Tahir, M. Iqbal, *Vibrio fischeri* bioluminescence inhibition assay for ecotoxicity assessment: a review, Sci. Total Environ., 626 (2018) 1295–1309.
[5] H. Shokry, M. Elkady, H. Hamad, Nano activated carbon from industrial mine coal as adsorbents for removal of dye from simulated textile wastewater: operational parameters and mechanism study, J. Mater. Res. Technol., 8 (2019) 4477–4488.
[6] M. Jafari, M. Reza Rahimi, M. Ghaedi, K. Dashtian, ZnO nanoparticles loaded different mesh size of porous activated carbon prepared from *Pinus eldarica* and its effects on simultaneous removal of dyes: multivariate optimization, Chem. Eng. Res. Des., 125 (2017) 408–421.
[7] M. Iqbal, *Vicia faba* bioassay for environmental toxicity monitoring: a review, Chemosphere, 144 (2016) 785–802.

[8] Z. Li, H. Hanafy, L. Zhang, L. Sellaoui, M.S. Netto, M.L.S. Oliveira, M.K. Seliem, G.L. Dotto, A. Bonilla-Petriciolet, Q. Li, Adsorption of congo red and methylene blue dyes on an ashitaba waste and a walnut shell-based activated carbon from aqueous solutions: experiments, characterization and physical interpretations, Chem. Eng. J., 388 (2020) 124263, https://doi.org/10.1016/j.cej.2020.124263.
[9] M. Kamaraj, N.R. Srinivasan, G. Assefa, A.T. Adugna, M. Kebede, Facile development of sunlit ZnO nanoparticles-activated carbon hybrid from pernicious weed as an operative nano-adsorbent for removal of methylene blue and chromium from aqueous solution: extended application in tannery industrial wastewater, Environ. Technol. Innovation, 17 (2020) 100540, https://doi.org/10.1016/j.eti.2019.100540.
[10] A.H. Jawad, R. Razuan, J.N. Appaturi, L.D. Wilson, Adsorption and mechanism study for methylene blue dye removal with carbonized watermelon (*Citrullus lanatus*) rind prepared *via* one-step liquid phase H_2SO_4 activation, Surf. Interfaces, 16 (2019) 76–84.
[11] U. Tyagi, Adsorption of dyes using activated carbon derived from pyrolysis of vetiveria zizanioides in a fixed bed reactor, Groundwater Sustainable Dev., 10 (2020) 100303, https://doi.org/10.1016/j.gsd.2019.100303.
[12] K.B. Daij, S. Bellebia, Z. Bengharez, Comparative experimental study on the COD removal in aqueous solution of pesticides by the electrocoagulation process using monopolar iron electrodes, Chem. Int., 3 (2017) 420–427.
[13] N. Oussama, H. Bouabdesselam, N. Ghaffour, L. Abdelkader, Characterization of seawater reverse osmosis fouled membranes from large scale commercial desalination plant, Chem. Int., 5 (2019) 158–167.
[14] A.M. Awwad, M.W. Amer, M.M. Al-Aqarbeh, TiO_2-kaolinite nanocomposite prepared from the Jordanian Kaolin clay: adsorption and thermodynamics of Pb(II) and Cd(II) ions in aqueous solution, Chem. Int., 6 (2020) 168–178.
[15] F. Minas, B.S. Chandravanshi, S. Leta, Chemical precipitation method for chromium removal and its recovery from tannery wastewater in Ethiopia, Chem. Int., 3 (2017) 392–405.
[16] K. Djehaf, A.Z. Bouyakoub, R. Ouhib, H. Benmansour, A. Bentouaf, A. Mahdad, N. Moulay, D. Bensaid, M. Ameri, Textile wastewater in Tlemcen (Western Algeria): impact, treatment by combined process, Chem. Int., 3 (2017) 414–419.
[17] M. Salari, M.H. Dehghani, A. Azari, M.D. Motevalli, A. Shabanloo, I. Ali, High performance removal of phenol from aqueous solution by magnetic chitosan based on response surface methodology and genetic algorithm, J. Mol. Liq., 2851 (2019) 146–157.
[18] L. Zhang, L. Sellaoui, D. Franco, G.L. Dotto, Z. Li, Adsorption of dyes brilliant blue, sunset yellow and tartrazine from aqueous solution on chitosan: analytical interpretation via multilayer statistical physics model, Chem. Eng. J., 38215 (2020) 122952, https://doi.org/10.1016/j.cej.2019.122952.
[19] E. Ayranci, O. Duman, *In-situ* UV-Visible spectroscopic study on the adsorption of some dyes onto activated carbon cloth, Sep. Sci. Technol., 44 (2009) 3735–3752.
[20] O. Duman, S. Tunç, T.G. Polat, B.K. Bozoğlan, Synthesis of magnetic oxidized multiwalled carbon nanotube-κ-carrageenan-Fe_3O_4 nanocomposite adsorbent and its application in cationic Methylene Blue dye adsorption, Carbohydr. Polym., 147 (2016) 79–88.
[21] O. Duman, T.G. Polat, C.Ö. Diker, S. Tunç, Agar/κ-carrageenan composite hydrogel adsorbent for the removal of Methylene Blue from water, Int. J. Biol. Macromol., 160 (2020) 823–835.
[22] S. Nekouei, F. Nekouei, Comparative procedure of photodegradation of methylene blue using N doped activated carbon loaded with hollow 3D flower like ZnS in two synergic phases of adsorption and catalytic, J. Photochem. Photobiol., A, 364 (2018) 262–273.
[23] X. Rong, F. Qiu, C. Zhang, L. Fu, D. Yang, Adsorption–photodegradation synergetic removal of methylene blue from aqueous solution by NiO/graphene oxide nanocomposite, Powder Technol., 275 (2015) 322–328.
[24] L. Sun, Q. Shao, Y. Zhang, H. Jiang, S. Ge, S. Lou, J. Lin, J. Zhang, S. Wu, M. Dong, Z. Guo, N self-doped ZnO derived from microwave hydrothermal synthesized zeolitic imidazolate framework-8 toward enhanced photocatalytic degradation of methylene blue, J. Colloid Interface Sci., 5651 (2020) 142–155.
[25] C.H. Nguyen, R.S. Juang, Efficient removal of methylene blue dye by a hybrid adsorption-photocatalysis process using reduced graphene oxide/titanate nanotube composites for water reuse, J. Ind. Eng. Chem., 7625 (2019) 296–309.
[26] M. Maruthupandy, T. Muneeswaran, M. Anand, F. Quero, Highly efficient multifunctional graphene/chitosan/magnetite nanocomposites for photocatalytic degradation of important dye molecules, Int. J. Biol. Macromol., 15315 (2020) 736–746.
[27] S. Cheng, Q. Chen, H. Xia, L. Zhang, J. Peng, G. Lin, X. Liao, X. Jiang, Q. Zhang, Microwave one-pot production of ZnO/Fe_3O_4/activated carbon composite for organic dye removal and the pyrolysis exhaust recycle, J. Cleaner Prod., 1881 (2018) 900–910.
[28] L.A. Calzada, R. Castellanos, L.A. García, T.E. Klimova, TiO_2, SnO_2 and ZnO catalysts supported on mesoporous SBA-15 vs. unsupported nanopowders in photocatalytic degradation of methylene blue, Microporous Mesoporous Mater., 2851 (2019) 247–258.
[29] M.F. Abdel Messih, M.A. Ahmed, A. Soltan, S. Sobhy Anis, Synthesis and characterization of novel Ag/ZnO nanoparticles for photocatalytic degradation of methylene blue under UV and solar irradiation, J. Phys. Chem. Solids, 135 (2019) 109086, https://doi.org/10.1016/j.jpcs.2019.109086.
[30] R.E. Adam, H. Alnoor, G. Pozina, X. Liu, M. Willander, O. Nur, Synthesis of Mg-doped ZnO NPs via a chemical low-temperature method and investigation of the efficient photocatalytic activity for the degradation of dyes under solar light, Solid State Sci., 99 (2020) 106053, https://doi.org/10.1016/j.solidstatesciences.2019.106053.
[31] W.S. Abo El-Yazeed, A.I. Ahmed, Photocatalytic activity of mesoporous WO_3/TiO_2 nanocomposites for the photodegradation of methylene blue, Inorg. Chem. Commun., 105 (2019) 102–111.
[32] O. Boura-Theodoridou, A. Giannakas, P. Katapodis, H. Stamatis, A. Ladavos, N.-M. Barkoula, Performance of ZnO/chitosan nanocomposite films for antimicrobial packaging applications as a function of NaOH treatment and glycerol/PVOH blending, Food Packag. Shelf Life, 23 (2020) 100456, https://doi.org/10.1016/j.fpsl.2019.100456.
[33] P. Falak, S.A. Hassanzadeh-Tabrizi, A. Saffar-Teluri, Synthesis, characterization, and magnetic properties of ZnO-$ZnFe_2O_4$ nanoparticles with high photocatalytic activity, J. Magn. Magn. Mater., 441 (2017) 98–104.
[34] Y. Xiao, H. Yu, X.-t. Dong, Ordered mesoporous CeO_2/ZnO composite with photodegradation concomitant photocatalytic hydrogen production performance, J. Solid State Chem., 278 (2019) 120893, https://doi.org/10.1016/j.jssc.2019.120893.
[35] S. Çınar, Ü.H. Kaynar, T. Aydemir, S. Çam Kaynar, M. Ayvacıklı, An efficient removal of RB5 from aqueous solution by adsorption onto nano-ZnO/Chitosan composite beads, Int. J. Biol. Macromol., 96 (2017) 459–465.
[36] D. Sharma, T. Singh, A DFT study of polyaniline/ZnO nanocomposite as a photocatalyst for the reduction of methylene blue dye, J. Mol. Liq., 2931 (2019) 111528, https://doi.org/10.1016/j.molliq.2019.111528.
[37] H. Atarodi, H. Faghihian, Selective photodegradation of atrazine by a novel molecularly imprinted nanophotocatalyst prepared on the basis of chitosan, J. Photochem. Photobiol., A, 3821 (2019) 111892, https://doi.org/10.1016/j.jphotochem.2019.111892.
[38] D. Tekin, H. Kiziltas, H. Ungan, Kinetic evaluation of ZnO/TiO_2 thin film photocatalyst in photocatalytic degradation of Orange G, J. Mol. Liq., 30615 (2020) 112905, https://doi.org/10.1016/j.molliq.2020.112905.
[39] M.H. Mostafa, M.A. Elsawy, M.S.A. Darwish, L.I. Hussein, A.H. Abdaleem, Microwave-assisted preparation of Chitosan/ZnO nanocomposite and its application in dye removal, Mater.

Chem. Phys., 248 (2020) 122914, https://doi.org/10.1016/j.matchemphys.2020.122914.
[40] O. Sacco, V. Vaiano, M. Matarangolo, ZnO supported on zeolite pellets as efficient catalytic system for the removal of caffeine by adsorption and photocatalysis, Sep. Purif. Technol., 19320 (2018) 303–310.
[41] H. Hassan, A. Salama, A.K. El-ziaty, M. El-Sakhawy, New chitosan/silica/zinc oxide nanocomposite as adsorbent for dye removal, Int. J. Biol. Macromol., 131 (2019) 520–526.
[42] W. Tie, Z. Zheng, C. Xu, Z. Zheng, S.H. Lee, Facile synthesis of carbon nanotubes covalently modified with ZnO nanorods for enhanced photodecomposition of dyes, J. Colloid Interface Sci., 5371 (2019) 652–660.
[43] B.A. Vessalli, C.A. Zito, T.M. Perfecto, D.P. Volanti, T. Mazon, ZnO nanorods/graphene oxide sheets prepared by chemical bath deposition for volatile organic compounds detection, J. Alloys Compd., 6965 (2017) 996–1003.
[44] M. Vinayagam, S. Ramachandran, V. Ramya, A. Sivasamy, Photocatalytic degradation of orange G dye using ZnO/biomass activated carbon nanocomposite, J. Environ. Chem. Eng., 6 (2018) 3726–3734.
[45] J. Saini, V.K. Garg, R.K. Gupta, N. Kataria, Removal of Orange G and Rhodamine B dyes from aqueous system using hydrothermally synthesized zinc oxide loaded activated carbon (ZnO-AC), J. Environ. Chem. Eng., 5 (2017) 884–892.
[46] A.H.A. Saad, A.M. Azzam, S.T. El-Wakeel, B.B. Mostafa, M.B. Abd El-latif, Removal of toxic metal ions from wastewater using ZnO@Chitosan core-shell nanocomposite, Environ. Nanotechnol. Monit. Manage., 9 (2018) 67–75.
[47] B.K. Bozoğlan, O. Duman, S. Tunç, Preparation and characterization of thermosensitive chitosan/carboxymethyl-cellulose/scleroglucan nanocomposite hydrogels, Int. J. Biol. Macromol., 162 (2020) 781–797.
[48] S.S. Al-Taweel, H.R. Saud, A.A.H. Kadhum, M.S. Takriff, The influence of titanium dioxide nanofiller ratio on morphology and surface properties of TiO_2/chitosan nanocomposite, Results Phys., 13 (2019) 102296, https://doi.org/10.1016/j.rinp.2019.102296.
[49] E.M. El Mouchtari, C. Daou, S. Rafqah, F. Najjar, H. Anane, A. Piram, A. Hamade, S. Briche, P. Wong-Wah-Chung, TiO_2 and activated carbon of *Argania Spinosa* tree nutshells composites for the adsorption photocatalysis removal of pharmaceuticals from aqueous solution, J. Photochem. Photobiol., A, 3881 (2020) 112183, https://doi.org/10.1016/j.jphotochem.2019.112183.
[50] F.I.M. Ali, S.T. Mahmoud, F. Awwad, Y.E. Greish, A.F.S. Abu-Hani, Low power consumption and fast response H_2S gas sensor based on a chitosan-CuO hybrid nanocomposite thin film, Carbohydr. Polym., 23615 (2020) 116064, https://doi.org/10.1016/j.carbpol.2020.116064.
[51] A.K. Prajapati, M.K. Mondal, Comprehensive kinetic and mass transfer modeling for methylene blue dye adsorption onto CuO nanoparticles loaded on nanoporous activated carbon prepared from waste coconut shell, J. Mol. Liq., 3071 (2020) 112949, https://doi.org/10.1016/j.molliq.2020.112949.
[52] H. Suo, L. Xu, C. Xu, H. Chen, D. Yu, Z. Gao, H. Huang, Y. Hu, Enhancement of catalytic performance of porcine pancreatic lipase immobilized on functional ionic liquid modified Fe_3O_4-Chitosan nanocomposites, Int. J. Biol. Macromol., 119 (2018) 624–632.
[53] R.S. Juang, Y.C. Yei, C.S. Liao, K.S. Lin, H.C. Lu, S.F. Wang, A.C. Sun, Synthesis of magnetic Fe_3O_4/activated carbon nanocomposites with high surface area as recoverable adsorbents, J. Taiwan Inst. Chem. Eng., 90 (2018) 51–60.
[54] R. Zhong, Q. Zhong, M. Huo, B. Yang, H. Li, Preparation of biocompatible nano-ZnO/chitosan microspheres with multi-functions of antibacterial, UV-shielding and dye photo-degradation, Int. J. Biol. Macromol., 1461 (2020) 939–945.
[55] N. Nasseh, F.S. Arghavan, S.R. Couto, A.H. Panahi, M. Esmati, T.J.A. Musawi, Preparation of activated carbon@ZnO composite and its application as a novel catalyst in catalytic ozonation process for metronidazole degradation, Adv. Powder Technol., 31 (2020) 875–885.
[56] Ch. Djilani, R. Zaghdoudi, P. Magri, F. Djazi, A. Lallam, B. Bouchekima, Elaboration and characterization of chitosan/banana peel biocomposite for the removal of dyes from wastewater, Desal. Water Treat., 151 (2019) 181–198.
[57] Ch. Djilani, R. Zaghdoudi, F. Djazi, B. Bouchekima, A. Lallam, A. Modarressi, M. Rogalski, Adsorption of dyes on activated carbon prepared from apricot stones and commercial activated carbon, J. Taiwan Inst. Chem. Eng., 53 (2015) 112–121.
[58] Ch. Djilani, R. Zaghdoudi, F. Djazi, B. Bouchekima, A. Lallam, P. Magri, Preparation and characterisation of activated carbon from animal bones and its application for removal of organic micropollutants from aqueous solution, Desal. Water Treat., 57 (2016) 25070–25079.
[59] L. Al-Naamani, S. Dobretsov, J. Dutta, J.G. Burgess, Chitosan-zinc oxide nanocomposite coatings for the prevention of marine biofouling, Chemosphere, 168 (2017) 408–417.
[60] M.M. Rao, G.P.C. Rao, K. Seshaiah, N.V. Choudary, M.C. Wang, Activated carbon from *Ceiba pentandra* hulls, an agricultural waste, as an adsorbent in the removal of lead and zinc from aqueous solutions, Waste Manage., 28 (2008) 849–858.
[61] F. Machda, T. Ogawa, H. Okumura, K.N. Ishihara, Damp-heat durability comparison of Al-doped ZnO transparent electrodes deposited at low temperatures on glass and PI-tape/PC substrates, Ceram. Int., 46 (2020) 16178–16184.
[62] M.S.E.M. Badawy, O.K.M. Riad, F.A. Taher, S.A. Zaki, Chitosan and chitosan-zinc oxide nanocomposite inhibit expression of *Las*I and *Rhl*I genes and quorum sensing dependent virulence factors of *Pseudomonas aeruginosa*, Int. J. Biol. Macromol., 14915 (2020) 1109–1117.
[63] B. Qiu, X. Xu, R. Deng, G. Xia, X. Shang, P. Zhou, Construction of chitosan/ZnO nanocomposite film by in situ precipitation, Int. J. Biol. Macromol., 122 (2019) 82–87.
[64] S.S. Narasagoudr, V.G. Hegde, R.B. Chougale, S.P. Masti, S. Dixit, Influence of boswellic acid on multifunctional properties of chitosan/poly(vinyl alcohol) films for active food packaging, Int. J. Biol. Macromol., 1541 (2020) 48–61.
[65] D. Sarabandi, G. Roudini, F. Barahuie, Activated carbon derived from pine cone as a framework for the preparation of n-heptadecane nanocomposite for thermal energy storage, J. Energy Storage, 24 (2019) 100795, https://doi.org/10.1016/j.est.2019.100795.
[66] M. Gharagozlou, S. Naghibi, Sensitization of ZnO nanoparticles by metal–free phthalocyanine, J. Lumin., 196 (2018) 64–68.
[67] M. Gharagozlou, S. Naghibi, Sensitization of ZnO nanoparticle by vitamin B12: investigation of microstructure, FTIR and optical properties, Mater. Res. Bull., 84 (2016) 71–78.
[68] P.M. Rahman, V.M.A. Mujeeb, K. Muraleedharan, S.K. Thomas, Chitosan/nano ZnO composite films: enhanced mechanical, antimicrobial and dielectric properties, Arabian J. Chem., 11 (2018) 120–127.
[69] P.M. Rahman, K. Muraleedaran, V.M.A. Mujeeb, Applications of chitosan powder with in situ synthesized nano ZnO particles as an antimicrobial agent, Int. J. Biol. Macromol., 77 (2015) 266–272.
[70] Z.I. Abdeen, A.F. El Farargy, N.A. Negm, Nanocomposite framework of chitosan/polyvinyl alcohol/ZnO: preparation, characterization, swelling and antimicrobial evaluation, J. Mol. Liq., 250 (2018) 335–343.
[71] I.V. Gala, J.L. Peñalve, M.S. Polo, J.R. Utrilla, Role of activated carbon surface chemistry in its photocatalytic activity and the generation of oxidant radicals under UV or solar radiation, Appl. Catal., B, 207 (2017) 412–423.
[72] M. Chen, C. Bao, D. Hu, X. Jin, Q. Huang, Facile and low-cost fabrication of ZnO/biochar nanocomposites from jute fibers for efficient and stable photodegradation of methylene blue dye, J. Anal. Appl. Pyrolysis, 139 (2019) 319–332.
[73] B. Bhushan, K. Jahan, V. Verma, B.S. Murty, K. Mondal, Photodegradation of methylene blue dye by powders of Ni–ZnO floweret consisting of petals of ZnO nanorod around Ni-rich core, Mater. Chem. Phys., 253 (2020) 123394, https://doi.org/10.1016/j.matchemphys.2020.123394.
[74] M. Mohsin, I.A. Bhatti, A. Ashar, A. Mahmood, Maryam, Q. ul Hassan, M. Iqbal, Fe/ZnO@ceramic fabrication for the enhanced photocatalytic performance under solar light irradiation for dye degradation, J. Mater. Res. Technol., 9 (2020) 4218–4229.

[75] A. Jamil, T.H. Bokhari, T. Javed, R. Mustafa, M. Sajid, S. Noreen, M. Zuber, A. Nazir, M. Iqbal, M.I. Jilani, Photocatalytic degradation of disperse dye Violet-26 using TiO_2 and ZnO nanomaterials and process variable optimization, J. Mater. Res. Technol., 9 (2020) 1119–1128.
[76] A. Jamil, T.H. Bokhari, M. Iqbal, M. Zuber, I.H. Bukhari, ZnO/UV/H_2O_2 based advanced oxidation of disperse red dye, Z. Phys. Chem., 234 (2019) 129–143.
[77] A. Inderyas, I.A. Bhatti, A. Ashar, M. Ashraf, A. Ghani, M. Yousaf, M. Mohsin, M. Ahmad, S. Rafique, N. Masood, Synthesis of immobilized ZnO over polyurethane and photocatalytic activity evaluation for the degradation of azo dye under UV and solar light irradiation, Mater. Res. Express, 7 (2020) 025033.
[78] S. Ata, I. Shaheen, Q. ul-Ayne, S. Ghafoor, M. Sultan, F. Majid, I. Bibi, M. Iqbal, Graphene and silver decorated ZnO composite synthesis, characterization and photocatalytic activity evaluation, Diamond Relat. Mater., 90 (2018) 26–31.
[79] J. Leichtweis, S. Silvestri, E. Carissimi, New composite of pecan nutshells biochar-ZnO for sequential removal of acid red 97 by adsorption and photocatalysis, Biomass Bioenergy, 140 (2020) 105648, https://doi.org/10.1016/j.biombioe.2020.105648.
[80] M.G. Gonçalves, P.A. da Silva Veiga, M.R. Fornari, P.P. Zamora, A.S. Mangrich, S. Silvestri, Relationship of the physicochemical properties of novel ZnO/biochar composites to their efficiencies in the degradation of sulfamethoxazole and methyl orange, Sci. Total Environ., 748 (2020) 141381, https://doi.org/10.1016/j.scitotenv.2020.141381.
[81] Sh. Sohrabnezhad, A. Seif, The green synthesis of Ag/ZnO in montmorillonite with enhanced photocatalytic activity, Appl. Surf. Sci., 386 (2016) 33–40.